American Mineralogist, Volume 89, pages 647–653, 2004

# A single-crystal study on the pressure behavior of phlogopite and petrological implications

P. COMODI,[1] P. FUMAGALLI,[2] M. MONTAGNOLI,[1] AND P.F. ZANAZZI[1,*]

[1]Dipartimento di Scienze della Terra, Università di Perugia, Piazza Università, I-06100 Perugia, Italy
[2]Dipartimento di Scienze della Terra, Università di Milano, Via Botticelli 23, I-20133 I-Milano, Italy

## ABSTRACT

The structural behavior of phlogopite was studied by in situ single-crystal X-ray diffraction (XRD) in a diamond-anvil cell, using crystals of composition $[(K_{0.91}Na_{0.02}Ba_{0.03})\ (Fe^{2+}_{0.65}Fe^{3+}_{0.163}Al_{0.123}Mg_{1.81}Ti_{0.149})Si_{2.708}Al_{1.292}O_{10}OH_{1.725}F_{0.175}]$. Lattice parameters were measured from 0.0001 to 6.5 GPa and fitted with a third-order Birch-Murnaghan equation of state (EoS). The resulting EoS parameters are: $V_0$ = 497.1(1) Å$^3$, $K_0$ = 54(2) GPa$^{-1}$, and $K'$ = 7(1); $a_0$ = 5.336(1) Å, $K_0$ = 123(9) GPa, and $K'$ = 3(2); $b_0$ = 9.240(3) Å, $K_0$ = 128(15) GPa, and $K'$ = 3(2); $c_0$ = 10.237(6) Å, $K_0$ = 25(2) GPa, and $K'$ = 5(1); the β angle increases linearly with pressure from 100.02(5) to 100.4(1)°.

The structural evolution of phlogopite was studied by comparing five structural refinements performed with intensity data collected at 0.0001, 1.2, 3.2, 5.0, and 6.0 GPa. The interlayer site, where K is located, is about 4.5 times more compressible than the T-O-T unit. At the same time, the greater compression of the octahedral layer with respect to the tetrahedral one induces an increase in tetrahedral rotation angle α from 9.29 to 11.9°.

Structural evolution with pressure yields a crystallographic rationale for the larger baric stability of K-deficient and Si-rich phlogopites, as observed from natural and experimental data.

Combined high-pressure and thermal expansion data yield the approximate EoS: $V = V_0(1 + 4.6 \times 10^{-5}\Delta T - 0.0167\ \Delta P)$, where $P$ is in GPa and $T$ in °C. This equation was used to calculate phase equilibria in lherzolite compositions modeled in the simplified $K_2O$-CaO-MgO-$Al_2O_3$-$SiO_2$-$H_2O$ (KCMASH) system. The results show that the effect of phlogopite on bulk density is particularly significant at high pressure and temperature since, above the chlorite stability field, phlogopite is the only hydrous phase able to lower bulk density properties by about 0.5% with respect to the K-free bearing system.

## INTRODUCTION

In recent years, many authors have investigated the stability range and decomposition of phlogopite. This mineral is expected to play an important role in mass transport and metasomatism occurring both along subducting slabs and within mantle wedges, as well as in melting processes, participating in the production of K-rich magma in the Earth's mantle. Both experimental data and geological evidence indicates that phlogopite is stable in upper mantle conditions.

Experiments on the stability of phlogopite as a pure phase reveal that it is stable up to 8–9 GPa (Trønnes 2002). Experimental data (Sudo and Tatsumi 1990) for phlogopite + diopside ± enstatite in the $K_2O$-CaO-MgO-$Al_2O_3$-$SiO_2$-$H_2O$ (KCMASH) system show that phlogopite can be stable up to 6–7 GPa and decomposes to K-amphibole + garnet + forsterite + fluid at higher pressures. Sato et al. (1997) investigated phase relations of both natural phlogopite and phlogopite + enstatite compositions. They suggested that phlogopite is stable in both compositions up to 5 GPa, at which point it breaks down to pyrope + $Al_2O_3$-deficient phlogopite + fluid. Experiments performed by Konzett and Ulmer (1999) on natural K-doped lherzolite systems suggest that phlogopite is stable up to 6.0–6.5 GPa at 1100 °C.

Recent discoveries of Ti-phlogopite in diamond-bearing inclusions in Bardane garnet peridotite intruded in subducted continental crust in Norway (van Roermund et al. 2002) support the key role of phlogopite in metasomatized mantle compositions at high pressure.

Although the crystal chemistry of phlogopite and its variations with pressure are still poorly known for ultramafic compositions, experimental results for felsic systems show that phlogopite compositions move toward talc through the exchange vector K + Al = □ + Si, rather than toward phengite (Hermann 2002). The importance of the talc component was also emphasized by Wunder and Melzer (2002), who investigated the concentration of interlayer vacancies as a function of composition in three synthetic series: K-Rb, K-Cs, and K-Ba solid solutions. Although the authors did not consider the effects of temperature and pressure, by combining infrared spectroscopy data and microprobe analysis, they found that interlayer vacancy concentration reaches 0.29 mol per formula unit.

The crystallographic mechanism of these substitutions and the crystal-chemical reasons for the stabilization of the talc component with pressure are not clear. Available data on the high-pressure structural behavior of phlogopite are restricted to the pioneering single-crystal study by Hazen and Finger (1978),

*E-mail: zanazzi@unipg.it

who reported only three data points for pressure and a structural refinement at 35(1) kbar. Pavese et al. (2003) recently performed synchrotron high-pressure powder diffraction experiments, but no high-pressure single-crystal study has been made recently.

In this study, we report the structural evolution of a natural phlogopite with pressure by analyzing different refinements and its compressibility up to 6.5 GPa. Our aim was to interpret the crystallographic reasons for the stabilization of the talc and/or phengitic component in the phlogopitic composition as pressure increases. We also aim to complete, as much as possible, the thermodynamic data set necessary for phase equilibrium calculations in mantle conditions. This will make it possible to evaluate density profiles involving phlogopite-bearing assemblages along a typical subduction path. The contribution of phlogopite to buoyancy forces is evaluated by comparing density profiles calculated for differently hydrated and K-enriched lherzolite compositions.

## Experimental methods

A natural sample of 1*M* phlogopite from the Colli Albani (Italy), whose crystal chemistry was investigated by Cruciani and Zanazzi (1994), was used for the high-pressure experiments. The average composition $[(K_{0.91}Na_{0.02}Ba_{0.03})(Fe^{2+}_{0.65}Fe^{3+}_{0.163}Al_{0.123}Mg_{1.81}Ti_{0.149})\ Si_{2.708}Al_{1.292}O_{10}OH_{1.725}F_{0.175}]$ corresponds to sample no. 4 studied by the same authors.

Unit-cell parameters and intensity data were determined using a Philips PW1100 four-circle diffractometer with graphite-monochromatized Mo$K\alpha$ radiation ($\lambda = 0.7107$ Å). A phlogopite crystal (Sample I) was mounted in a Merrill-Basset diamond-anvil cell (DAC) together with crystals of $Sm^{2+}$: BaFCl and quartz. The pressure chamber was a hole of diameter 300 μm in a steel gasket 0.25 mm thick. A methanol-ethanol mixture (4:1) was used as the pressure-transmitting medium. The wavelength shift of the 6876 Å $Sm^{2+}$ fluorescence line, excited by a 100 mW Ar laser and detected by a 100 cm Jarrell-Ash optical spectrometer, was measured for an approximate estimate of pressure (Comodi and Zanazzi 1993); the effective pressure was measured with the quartz crystal (Angel et al. 1997). Uncertainties in pressure measurements were assumed to be of the order of 0.05 GPa. To improve the data set, a second crystal was mounted (Sample II). Unit-cell parameters were determined in the pressure range 0.0001 to 6.5 GPa (Table 1), through the θ angles of 30 reflections accurately centered in several equivalent positions on the diffractometer. Intensity data were collected in the range 3–35° θ with 2.8° wide ω scans, at pressures of 0.0001, 1.2, 3.2, 5.0, and 6.0 GPa, using non-bisecting geometry (Denner et al. 1978), in order to maximize reflection accessibility and minimize attenuation of the X-ray beam by the DAC components. The data were analyzed with a digital procedure (Comodi et al. 1994) and were corrected for pressure-cell absorption with an experimental attenuation curve (Finger and King 1978).

Crystal structure refinements were made with the SHELX-97 program (Sheldrick 1997) in space group *C*2/*m*. Isotropic atomic displacement parameters were used for all atoms. Neutral atomic scattering factors values were taken from the *International Tables for X-ray Crystallography* (Ibers and Hamilton 1974). The occupancy factors for the M1 and M2 sites were refined assuming full occupancy of Mg and Fe; the results of the refinements gave 72% Mg at M1 and 73% Mg at M2, consistent with the chemical analysis. Details of data collection and refinement are listed in Table 2. The data at 0.0001 GPa were collected with the sample mounted in the DAC in order to avoid systematic errors when comparing the refinement results obtained using reflections measured under room conditions belonging to the whole reciprocal lattice with results obtained with reflections measured from a limited part of the reciprocal space within the DAC. Fractional atomic coordinates and displacement parameters are listed in Table 3[1] and observed and calculated structure factors in Table 4[1].

[1] For a copy of Tables 3 and 4, Documents AM-04-063, contact the Business Office of the Mineralogical Society of America (see inside cover of a recent issue for price information). Deposit items may also be available on the American Mineralogist web site at http://www.minsocam.org.

**Table 1.** Lattice parameters of phlogopite at various pressures

| *P* (GPa) | *a* (Å) | *b* (Å) | *c* (Å) | *V* (Å) | β (°) |
|---|---|---|---|---|---|
| | | | **Sample I** | | |
| 0.0001 | 5.337(2) | 9.240(3) | 10.237(6) | 497.1(1) | 100.02(5) |
| 0.9 | 5.322(2) | 9.222(9) | 10.13(1) | 489.5(3) | 100.10(5) |
| 1.2 | 5.318(2) | 9.210(9) | 10.10(2) | 487.0(4) | 100.12(8) |
| 2.7 | 5.300(2) | 9.183(9) | 9.95(2) | 476.6(4) | 100.2(1) |
| 3.2 | 5.291(2) | 9.160(9) | 9.90(1) | 472.1(6) | 100.3(1) |
| 3.62 | 5.286(1) | 9.161(8) | 9.88(2) | 470.8(4) | 100.3(1) |
| 5.0 | 5.271(2) | 9.130(9) | 9.78(2) | 463.0(3) | 100.3(1) |
| 6.0 | 5.256(1) | 9.105(9) | 9.71(2) | 457.0(4) | 100.4(1) |
| 6.5 | 5.252(2) | 9.096(8) | 9.68(2) | 454.8(4) | 100.4(1) |
| | | | **Sample II** | | |
| 2.15 | 5.307(2) | 9.186(8) | 9.99(1) | 479.2(2) | 100.24(7) |
| 3.0 | 5.298(3) | 9.172(9) | 9.94(3) | 475.3(5) | 100.23(8) |
| 3.95 | 5.284(4) | 9.150(6) | 9.86(1) | 469.0(3) | 100.31(9) |
| 4.3 | 5.278(3) | 9.140(7) | 9.83(1) | 466.6(3) | 100.26(9) |
| 4.75 | 5.272(2) | 9.13(1) | 9.80(1) | 464.1(3) | 100.3(1) |
| 5.2 | 5.267(2) | 9.12(1) | 9.77(2) | 461.6(4) | 100.38(9) |
| 5.78 | 5.260(4) | 9.11(1) | 9.72(2) | 458.1(5) | 100.38(8) |

**Table 2.** Details of data collection and refinement at various pressures

| *P* (GPa) | 0.0001* | 1.2 | 3.2 | 5.0 | 6.0 |
|---|---|---|---|---|---|
| N. refl. | 1227 | 1213 | 1195 | 1158 | 1130 |
| N. of unique refl. | 258 | 300 | 286 | 304 | 353 |
| N. of observed refl. | 190 | 207 | 217 | 226 | 244 |
| N. refined par. | 30 | 30 | 30 | 30 | 30 |
| $R_{eq}$% | 4.5 | 7.5 | 7.7 | 6.5 | 6.4 |
| *R*% (*F*) | 7.1 | 6.2 | 6.1 | 4.8 | 4.8 |

* Data collected under room conditions with crystal in the DAC without a pressure medium.

## Results

### Compressibility and *P-V-T* equation of state

Unit-cell parameter variations with *P* (Table 1) are shown in Figure 1. The plot of "normalized stress" vs. the Eulerian finite strain (Angel 2000) (Fig. 2) confirms that a third-order truncation appropriately describes the measured data. Therefore, volume-pressure data were fitted with a third-order Birch-Murnaghan Equation of State (EoS). The resulting EoS parameters were $V_0 = 497.1(1)$ Å$^3$, very close to the measured value, $K_0 = 54(2)$ GPa$^{-1}$, and $K' = 7(1)$ (Table 1).

The bulk modulus obtained by Hazen and Finger (1978), corresponding to 58.5 ± 2.0 GPa, is in fair agreement with our value. Pavese et al. (2003) recently studied the compressibility of phlogopite with synchrotron powder diffraction and obtained $K_0 = 49.7$ (±0.5) GPa, with $K' = 8.59$ (±0.19).

The "axial moduli" measured along the cell edges were obtained by fitting a "linearized" third-order Birch-Murnaghan EoS (Angel 2000), simply by substituting the cube of the lattice parameter for the volume. The results were $a_0 = 5.336(1)$ Å, $K_0 = 123(9)$ GPa, and $K' = 3(2)$; $b_0 = 9.240(3)$ Å, $K_0 = 128(15)$ GPa, and $K' = 3(2)$; $c_0 = 10.237(6)$ Å, $K_0 = 25(2)$ GPa, and $K' = 5(1)$. As expected, the phlogopite compressional pattern is strongly anisotropic. The axial compressibility values, obtained by dividing the inverse of the axial moduli by three, were $\beta_{0\mathbf{a}}^{EoS} = 2.7(2)$, $\beta_{0\mathbf{b}}^{EoS} = 2.6(1)$, and $\beta_{0\mathbf{c}}^{EoS} = 13.3(2)\ 10^{-3}$ GPa$^{-1}$, which represent intermediate values with respect to previous data. Pavese et al. (2003) obtained axial compressibilities of $\beta_{0\mathbf{a}}^{EoS} = 3.48(5)$, $\beta_{0\mathbf{b}}^{EoS} = 3.2(1)$, and $\beta_{0\mathbf{c}}^{EoS} = 13.2(1)\ 10^{-3}$ GPa$^{-1}$; the data of Hazen and Finger (1978), fitted with a second-order Birch-Murnaghan EoS, give $\beta_{0\mathbf{a}}^{EoS} = 2.69(5)$, $\beta_{0\mathbf{b}}^{EoS} = 2.99(2)$, and $\beta_{0\mathbf{c}}^{EoS} = 15.1(9)\ 10^{-3}$ GPa$^{-1}$. As previously observed for other micas and layer silicates, the most

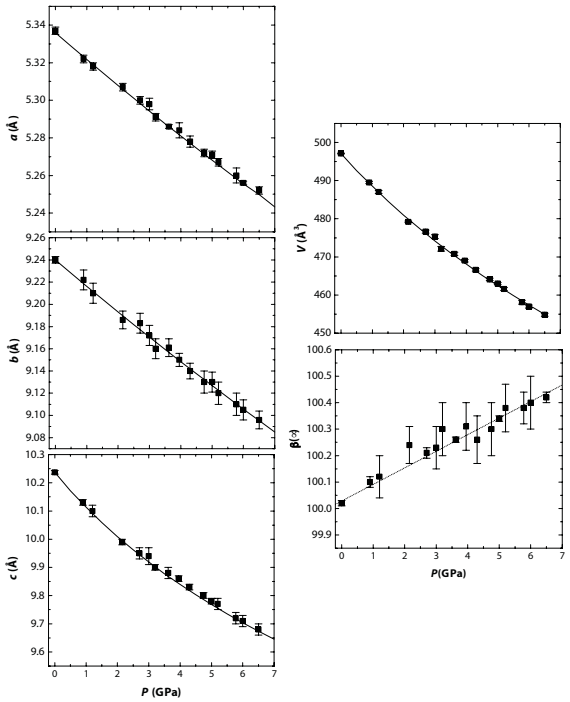


**FIGURE 1**. Variations in lattice parameters of phlogopite as a function of pressure. Solid curves: Birch-Murnaghan EoS best fit. Dotted curve: linear fit of β angle.

pronounced pressure effect relies on the **c** axis and is related to the particular structure.

Tutti et al. (2000) studied the thermal expansion of a natural phlogopite sample using X-ray powder diffraction data collected up to 1050 °C, in order to determine the dehydroxylation mechanism and the stability limits of this phase. At first approximation, we can consider the effects of *P* and *T* to be approximately inverse, in an attempt to define an approximate equation of state for phlogopite. We can write the following EoS for phlogopite by combining our *P*-*V* data with the *T*-*V* data measured by Tutti et al. (2000): $V = V_0 (1 + 4.6 \times 10^{-5} \Delta T - 0.0167 \Delta P)$, where *P* is in GPa and *T* in °C.

### Structural evolution with *P*

Intensity data from crystals mounted in a DAC are always affected by systematic errors stemming from various interactions of the X-ray beam with the components of the cell. The effects of pressure on the phlogopite structure were therefore studied by comparing the structural refinements performed with data collected at 1.2, 3.2, 5.0, and 6.0 GPa with those performed with data collected at 0.0001 GPa, with the sample mounted in the DAC. Variations in bond distances and polyhedral volumes with *P* are listed in Table 5. Figure 3 shows the mean polyhedral bond distances, normalized to the ambient condition value, against *P*. The evolution of the volume polyhedra with *P* was fitted linearly; this approximation was considered appropriate owing to the small number of data points. Single polyhedral bulk moduli were calculated as the reciprocals of the mean compressibility coefficients taken from the linear fits. Comparison of the results shows that, in the investigated range, the tetrahedra are almost incompressible, whereas the M1 and M2 octahedra have bulk moduli of 87(8) and 85(8) GPa, respectively.

The tetrahedral rotation angle (α) increases with pressure from 9.3 to 11.9°; this is necessary to facilitate dimensional matching between the tetrahedral and octahedral sheets due to their different compressibilities.

At the same time, both longer and shorter <K-O> (Å) bond lengths decrease roughly linearly with pressure, and the increase in the α angle leads to greater differences: $<K\text{-}O>_{inner}$ decreases with pressure more rapidly than $<K\text{-}O>_{outer}$ (Fig. 4).

The mica structure is composed of overlapping tetrahedral-octahedral-tetrahedral (T-O-T) sheets linked by an interlayer cation. These structural units behave differently under compression. The most evident response to pressure is from the interlayer, where K is located and where the charge density is lowest. The bulk moduli of the interlayer and T-O-T units are 37(3) and 167(28) GPa, respectively, the interlayer being about 4.5 times more compressible than the T-O-T units. Data on the variations in tetrahedral and octahedral sheets and interlayer thickness are listed in Table 5.

### Petrological implications

In subduction zones potassium-bearing metasomatizing fluids may interact with mantle peridotite, leading to the formation of phlogopite both within mantle wedges and along the mantle-slab interface. Phlogopite is expected to affect ultramafic bulk density significantly, playing an important role in controlling buoyancy forces and dynamics acting at convergent margins.

In order to explore the contribution of phlogopite to buoyancy forces in subduction zones, phase diagrams for differently hydrated and K-enriched lherzolite compositions were calculated using the PeRpLeX packages (Connolly 1990), taking advantage of the equation of state of phlogopite obtained in this study. The Tinaquillo lherzolite was considered as the model bulk composition and, rescaled to the simplified $CaO\text{-}MgO\text{-}Al_2O_3\text{-}SiO_2$ (CMAS) system and on a anhydrous and K-free basis, gives the following percentages: CaO = 3.02, MgO = 48.24, $Al_2O_3$ = 3.26, and $SiO_2$ = 45.47 wt%. According to the phase assemblages obtained at fixed compositions, PeRpLeX defines bulk density profiles along a geotherm (Connolly and Petrini 2002). In this study, a gradient of 125 K/GPa was chosen as representative of a typical subduction path (Kincaid and Sacks 1997). The internally consistent thermodynamic database of Holland and Powell (1998, and subsequent upgrades) was used for all phases except phlogopite, whose EoS was substituted with that obtained in this study. As such a procedure would invalidate the principle of the so-called "internal consistency", the EoS derived in this work was expected to affect phase relations only at high pressure, conditions at which no data on phlogopite can be retrieved. The Holland and Powell database takes into account data obtained at pressures under 12 kbar (Aranovich and Newton 1998). Ultramafic compositions were modeled in the simplified chemical system $K_2O\text{-}CaO\text{-}MgO\text{-}Al_2O_3\text{-}SiO_2\text{-}H_2O$ (KCMASH). As a result, solid solutions permitted and considered in the calculations involve the Tschermak exchange in pyroxene (Ca-tschermak in clinopyroxene, Gasparik 1984; and Mg-tschermak in orthopyroxene, Holland and Powell 1998) and

**TABLE 5.** Interatomic distances and geometric parameters in phlogopite

| *P* (GPa) | 0.0001* | 1.2 | 3.2 | 5.0 | 6.0 |
|---|---|---|---|---|---|
| α (°) | 9.3(3) | 10.5(2) | 11.4(4) | 12.0(3) | 11.9(4) |
| Δ*z* (Å) † | –0.02(1) | –0.02(1) | –0.02(1) | –0.02(1) | –0.02(1) |
| $V_T$ (Å$^3$) | 2.4(1) | 2.3(1) | 2.4(1) | 2.3(1) | 2.4(2) |
| <T-O> (Å) | 1.67(2) | 1.66(3) | 1.67(2) | 1.65(2) | 1.67(2) |
| Tetrahedral sheet thickness (Å) | 2.25 | 2.21 | 2.26 | 2.22 | 2.29 |
| $V_{M1}$ (Å$^3$) | 12.0(4) | 11.9(3) | 11.7(3) | 11.6(4) | 11.1(7) |
| $V_{M2}$ (Å$^3$) | 11.9(4) | 11.8(4) | 11.6(4) | 11.5(6) | 11.0(6) |
| <M1-O> (Å) | 2.09(3) | 2.08(2) | 2.07(2) | 2.06(3) | 2.04(3) |
| <M2-O> (Å) | 2.09(2) | 2.08(1) | 2.07(2) | 2.06(2) | 2.03(3) |
| Octahedral sheet thickness (Å) | 2.20 | 2.18 | 2.16 | 2.15 | 2.08 |
| $\psi_{M1}$(°) | 58.5(3) | 58.5(2) | 58.6(1) | 58.6(3) | 59.4(5) |
| $\psi_{M2}$(°) | 58.4(3) | 58.4(2) | 58.5(1) | 58.5(5) | 59.3(5) |
| <K-$O_{inner}$> (Å) | 2.95(3) | 2.90(3) | 2.80(4) | 2.76(3) | 2.73(4) |
| <K-$O_{outer}$> (Å) | 3.38(3) | 3.39(3) | 3.34(4) | 3.33(4) | 3.30(4) |
| Δ(K-O) (Å) | 0.43(4) | 0.48(4) | 0.54(6) | 0.56(5) | 0.57(6) |
| K-OH (Å) | 3.92 (3) | 3.88(3) | 3.73(4) | 3.72(3) | 3.70(4) |
| $V^{XII}$ (Å$^3$) | 81.0(2) | 79.4(2) | 73.5(1) | 71.3(3) | 68.7(4) |
| $V^{VI}$ (Å$^3$) | 34.3(2) | 32.6(2) | 29.3(2) | 28.0(3) | 26.9(3) |
| Interlayer thickness (Å) | 3.39 | 3.34 | 3.11 | 3.03 | 2.94 |

* Data collected under room conditions with crystal in the DAC without a pressure medium.
† Δ*z* was calculated as $[(z_{O1'} + z_{O1})/2 - z_{O2}]\ c \sin\beta$ (Guven 1971).

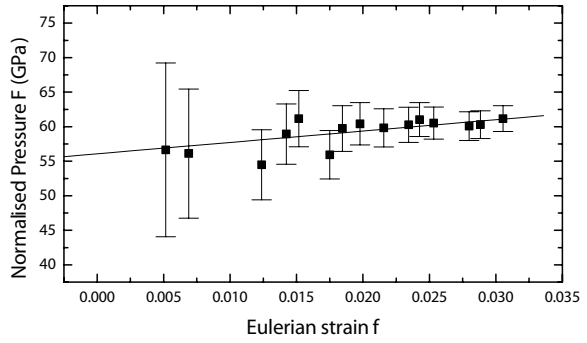


**FIGURE 2.** Plot of "normalized stress," defined as $F_E = P / [3f_E(1 + 2f_E)^{5/2}]$, vs. finite strain $f_E = [(V_0 / V)^{2/3} - 1]/2$.

the $CaMg_{-1}$ exchange in garnet (pyrope-grossular solid solution, Holland and Powell 1998).

The effects of hydrogen and potassium on bulk density profiles were identified by considering differing compositions ranging from a dry, K-free ($H_2O$ = 0.0 wt%, $K_2O$ = 0.0 wt%) through a hydrated, K-free ($H_2O$ = 0.5, 1.0 wt%), to a hydrated, K-bearing lherzolite ($H_2O$ = 0.5, 1.0 wt%, $K_2O$ = 0.5 wt%). The results of the calculations are shown in Figure 5.

Phase assemblages for the model anhydrous lherzolite consist of olivine (ca. 67.0 vol%), orthopyroxene (9.7–18.8 vol%), clinopyroxene (9.2–11.5 vol%), and spinel (2.3–2.5 vol%) or garnet (7.5–10.5 vol%), depending on pressure. The density profile shows a discontinuity (number 1 in Fig. 5) at the spinel-to-garnet transition which, at ≈1.6 GPa, leads to about 0.5% denser ultramafic assemblages.

As hydrogen and potassium are added to the system, hydrous phases such as chlorite and phlogopite form, strongly affecting phase equilibria, phase abundances and, consequently, bulk density. Among the phases, those with aluminum, i.e., spinel and garnet, are most influenced by phlogopite and chlorite; changes in their abundances have a profound effect on bulk density. In order to better evaluate the effect of chlorite and phlogopite, the

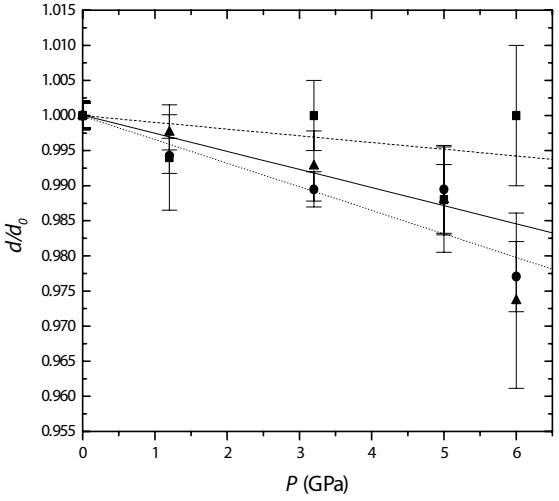


**FIGURE 3.** Mean polyhedral bond distances normalized to room condition value vs. pressure. Solid squares and dashed line refer to T; solid triangles and solid line refer to M2; solid circles refer to M1.

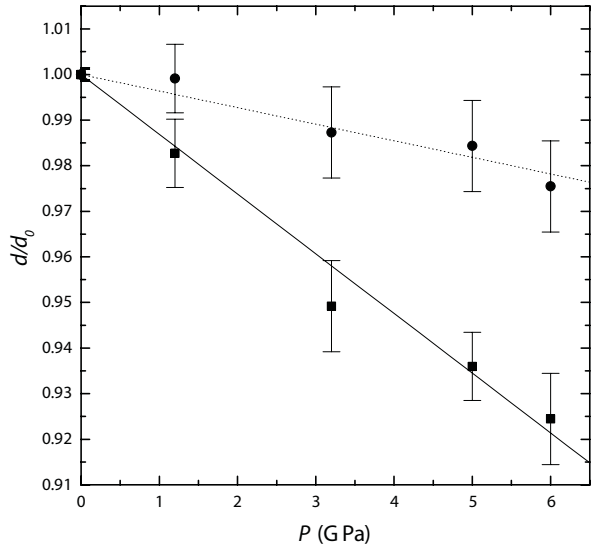


**FIGURE 4.** Mean K-O bond distances normalized to room condition value vs. pressure. Full squares and solid line refer to <K-O>$_{inner}$; full circles and dotted line refer to <K-O>$_{outer}$.

hydrous, K-free system (CMASH) is discussed first.

Chlorite (assumed to be of clinochlore composition) makes up about 4.6 vol% of the whole phase assemblage for $H_2O$ = 0.5 wt% and 9.2 vol% for $H_2O$ = 1.0 wt%. For a fixed $H_2O$ content (1.0 wt%), spinel modal abundance is reduced to 0.5–0.7 vol% and garnet to 1.8–2.8 vol%. As pressure increases, chlorite breaks down and an anhydrous assemblage (olivine, orthopyroxene, clinopyroxene, and garnet) coexists with a fluid. A discontinuity in the density profile, indicated as number 2 in Figure 5, identifies the "chlorite-out" reaction at about 3.3 GPa, leading to an increase in bulk density of about 1.4 and 2.5% for $H_2O$ contents of 0.5 and 1.0 wt%, respectively. Fluid present at pressure and temperature conditions above the stability of chlorite was not

taken into account for bulk density calculations, as it was assumed that fluids escape from the system. As a result, since no hydrates are stable above the chlorite stability field, the bulk density profile for the hydrous K-free composition under these pressure and temperature conditions is not affected by hydrogen and coincides with that found for dry conditions. The overall effect of hydrogen on bulk density is therefore appreciable only within the stability field of chlorite and is estimated as a decrease of about 0.9% for each 0.5 wt% of $H_2O$ added to the system.

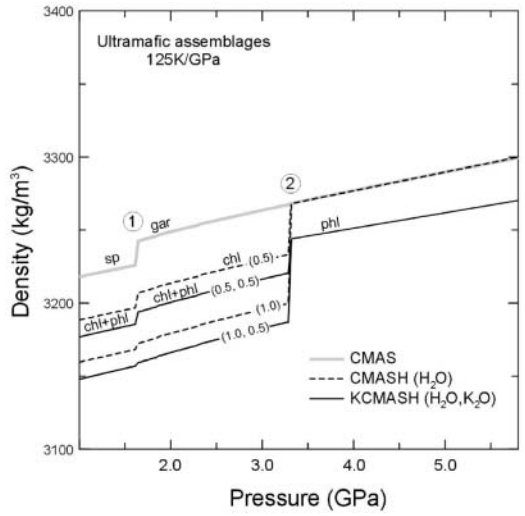


**FIGURE 5.** Bulk density profiles for lherzolite phase assemblages along a geotherm of 125K/GPa. In gray: density profile for a dry, K-free system (CaO-MgO-$Al_2O_3$-$SiO_2$, CMAS); dashed lines: CMAS-$H_2O$ (CMASH) system (values between brackets indicate the wt% of $H_2O$ considered); solid lines: $K_2O$-CMASH (KCMASH) system (values in brackets: wt% of $H_2O$ and $K_2O$ respectively); 1 and 2: spinel-to-garnet transition and "chlorite-out" reaction respectively. Sp: spinel; gar: garnet; chl: chlorite; phl: phlogopite.

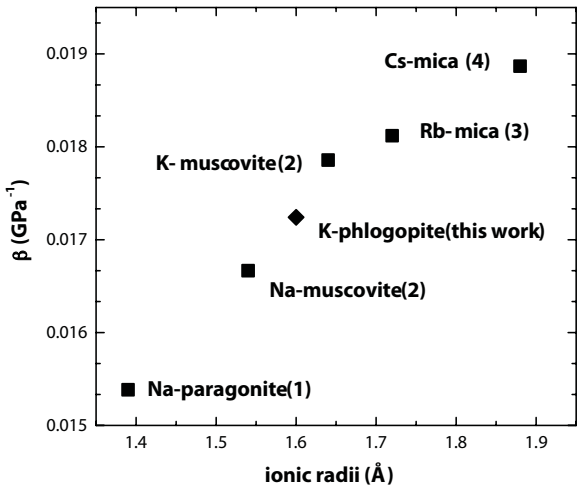


**FIGURE 6.** Compressibility of some micas vs. ionic radii of the interlayer cation (radii from Shannon 1976). (1) Na-paragonite (Comodi and Zanazzi 1997); (2) Na-muscovite and K-muscovite (Comodi and Zanazzi 1995); (3) Rb-mica (Comodi et al. 2003); (4) Cs-mica (Comodi et al. 1999).

In the K-bearing system ($K_2O$ = 0.5 wt%), phase assemblages are similar to those previously described, except for the ubiquitous occurrence of phlogopite (5.0 vol%), which has the effect of further reducing abundances of the Al-bearing phases: chlorite is reduced to 7.4 vol% for $H_2O$ = 1.0 and to 2.9 vol% for $H_2O$ = 0.5, and spinel to 1.1–1.3 ($H_2O$ = 0.5 wt%) and 0.3–0.5 vol% ($H_2O$ = 1.0 wt%). Garnet abundance reduction is particularly significant when garnet coexists with phlogopite alone, i.e., above the "chlorite-out" reaction, reaching values 25% lower than in either dry or hydrous K-free compositions. As expected, up to the pressure and temperature conditions at which chlorite is stable and coexists with phlogopite, the effect of potassium is combined with that of hydrogen, leading to an overall decrease in bulk density ranging from 1.5 to 2.5% for $H_2O$ = 0.5 and 1.0 wt%, respectively. An important discontinuity on the bulk density profile appears at the "chlorite-out" reaction, which leads to phlogopite coexisting with a fluid (for both 0.5 and 1.0 wt% $H_2O$).

Density profiles previously discussed are consistent with density profiles calculated by considering other available EoS, namely: (1) the EoS presently available in the Holland and Powell database (1998); (2) the EoS from Pavese et al. (2003); and (3) the EoS derived from the results of Hazen and Finger (1978). Indeed, differences in the density profiles are mainly controlled by differences in cell volumes. The Holland and Powell (1998) database gives a volume for phlogopite of 497.10 Å$^3$, which is comparable with the volume obtained in this study (497.08 Å$^3$). Although Pavese et al. (2003) and Hazen and Finger (1978) reported cell volumes which are 1.7–1.9% smaller (488.64 and 487.70 Å$^3$, respectively), such a percentage results in a negligible difference in the bulk density, which has been evaluated to less than 0.1%.

## DISCUSSION

We investigated the pressure dependence of the structure and compressibility of phlogopite, and make the following comments:

(1) Although it is expected that the composition of phlogopite is controlled as pressure increases by the cation substitution Al + Al = Mg + Si (*phengitic substitution*), Hermann (2002) suggested that pressure also favors the solid solution of phlogopite toward talc, following the exchange vector: K + Al = □ + Si (*K-edenitic substitution*). These substitutions have the combined effect of reducing the α rotation by decreasing the dimensions of the tetrahedral layer, coupled in the phengitic substitution by an increase in the octahedral layer. Our experimental data shows that the main distortion mechanism that phyllosilicates may undergo as a consequence of increasing pressure regards tetrahedral rotation. This is due to the misfit induced by the greater compressibility of the octahedral layer with respect to the tetrahedral layer, which may be compensated for through tetrahedral rotation.

However, the increase in α with pressure leads to destabilization of the mica structure. Too large an α rotation could push the tetrahedral and octahedral cations together, increasing electrostatic energy (Griffen 1992). As a result, those crystal-chemical

mechanisms which reduce α rotation determine those structures able to support greater pressures.

In the case of the K-edenitic substitution, which involves a large talc component under high-pressure conditions, the present study gives another crystal-chemical reason to explain the α rotation. Repulsion between interlayer cation and hydroxyl is documented by crystal-chemical studies, which have shown how the interaction between interlayer cations and protons increases the separation between adjacent 2:1 layers. In particular, Bailey (1984) described how this effect is mitigated in dioctahedral micas, where the O-H vector does not point directly toward the interlayer cation, but is directed toward the octahedral vacant site. Instead, in trioctahedral micas, the interlayer cation lies near the H atom of the OH group, because the proton is equidistant from the three octahedral cations and the O-H vector is nearly vertical to the (001) plane. The present study shows that the greater reduction affects interlayer thickness (Table 5) and, as a consequence, the distance between interlayer cation and hydroxyl groups is greatly reduced (e.g., the K-OH distance changes from 3.92 Å at room conditions to 3.70 Å at 6.0 GPa, Table 5), and the repulsive force is greatly increased. The K +Al = □ + Si mechanism, which reduces the interlayer charge, therefore decreases the repulsive term, especially under high-pressure conditions.

A similar mechanism that can to reduce the repulsion between hydroxyl units and interlayer cations is the substitution of fluorine for OH. This mechanism has been invoked to explain the greater thermal stability of F-rich trioctahedral micas with respect to F-poor micas (Brigatti and Guggenheim 2002).

In amphiboles the same mechanism is invoked by Comodi et al. (1991) to explain the natural observation that F-amphiboles have a greater pressure stability than hydroxyl-amphiboles. Also in that case, the repulsive effect due to the reduced distance between the hydrogen atom and the A cation under high pressure is mitigated by the substitution of the fluorine atom instead of the hydroxyl group.

(2) Ferraris and Ivaldi (2002) pointed out that the increase in tetrahedral rotation angle α causes the coordination of the interlayer cation to change from [XII] to [VI+VI], suggesting that the T-O-T unit plays an important role in the whole compressional behavior of mica.

To better understand the roles of the interlayer cations and the T-O-T package, we compared the high-pressure behavior of some trioctahedral and dioctahedral micas studied in our laboratory by plotting the compressibility coefficient against the ionic radii of the interlayer cation. The common trend occurring in both di- and tri-octahedral micas (Fig. 6) suggests that the interlayer cation strongly controls bulk mica compressibility. Tetrahedral tilting, previously observed for several silicates as a consequence of increasing pressure, represents a preferential way, from an energy point of view, of reducing the misfit induced by the differing compressibilities of the tetrahedral and octahedral sheets, but the size of the interlayer cation in the mica structure determines the actual evolution of this mechanism.

(3) The results of phase equilibria calculated for ultramafic compositions modeled in a simplified KCMASH system, using the equation of state defined above and the PeRpLEX packages, show that the effect of phlogopite on bulk density is particularly significant at high pressure and temperature, since it is the only hydrate stable in these conditions which is able to lower bulk density properties. At pressures higher than the "chlorite-out reaction", the phlogopite-bearing system has a bulk density lower by about 0.5% than the K-free system.

## ACKNOWLEDGMENTS

The authors are grateful to J.A.D. Connolly and S. Poli for their useful comments and suggestions. This work was supported by Italian C.N.R and M.U.R.S.T grants to P.F.Z. The English text was revised by G. Walton.

## REFERENCES CITED

Angel, R.J. (2000) Equations of state. In R.M. Hazen and R.T. Downs, Eds., High-Temperature and High-pressure Crystal Chemistry. Reviews in Mineralogy and Geochemistry, 41, 35–59. Mineralogical Sociey of America and the The Geochemical Society, Washington, D.C.

Angel, R.J., Allan, D.R., Miletich, R., and Finger, L.W. (1997) The use of quartz as an internal pressure standard in high pressure crystallography. Journal of Applied Crystallography, 30, 461–466.

Aranovich, L.Y. and Newton, R.C. (1998) Reversed determination of the reaction: Phlogopite + quartz = enstatite + potassium feldspar + $H_2O$ in the ranges 750–875 °C and 2–12 kbar at low $H_2O$ activity with concentrated KCl solutions. American Mineralogist, 83, 193–204.

Bailey, S.W. (1984) Crystal chemistry of the true micas. In S.W. Bailey, Ed., Micas. Reviews in Mineralogy, 13, 13–60. Mineralogical Society of America, Washington, D.C.

Brigatti, M.F. and Guggenheim, S. (2002) Mica crystal chemistry and the influence of pressure, temperature and solid solution on atomistic models. In A. Mottana, F.P. Sassi, J.B. Thompson, Jr., S. Guggenheim, Eds., Micas: Crystal Chemistry and Metamorphic Petrology. Reviews in Mineralogy and Geochemistry, 46, 1–97. The Italian National Academy, the Geochemical Society, and the Mineralogical Sociey of America, Washington, D.C.

Comodi, P. and Zanazzi, P.F. (1993) Improved calibration curve for the $Sm^{2+}$:BaFCl pressure sensor. Journal of Applied Crystallography, 26, 843–845.

——— (1995) High-pressure study of muscovite. Physics and Chemistry of Minerals, 22, 170–177.

——— (1997) Pressure dependence of structural parameters of paragonite. Physics and Chemistry of Minerals, 24, 274–280.

Comodi, P., Mellini, M., Ungaretti L., and Zanazzi P.F. (1991) Compressibility and high pressure structure refinement of tremolite, pargasite and glaucophane. European Journal of Mineralogy, 3, 485–499.

Comodi, P., Melacci, P.T., Polidori, G., and Zanazzi P.F. (1994) Trattamento del profilo di diffrazione da campioni in cella ad alta pressione. Proceedings of XXIV National Congress of the Associazione Italiana di Cristallografia. Pavia, 27–29 September, 119–120.

Comodi, P., Zanazzi, P.F., Weiss, Z., Rieder, M., and Drábek, M. (1999) "Cs-tetra-ferri-annite": high-pressure and high-temperature behaviour of a potential nuclear waste disposal phase. American Mineralogist, 84, 325–332.

Comodi, P., Drábek, M., Montagnoli, M., Rieder, M., Weiss, Z., and Zanazzi, P.F. (2003) Pressure-induced phase transition in synthetic trioctahedral Rb-mica. Physics and Chemistry of Minerals, 30, 198–205.

Connolly, J.A.D. (1990) Multivariable phase diagrams: an algorithm based on generalized thermodynamics. American Journal of Science, 290, 666–718.

Connolly, J.A.D. and Petrini, K. (2002) An automated strategy for calculation of phase diagram sections and retrieval of rock properties as a function of physical conditions. Journal of Metamorphic Geology, 20, 697–708.

Cruciani, G. and Zanazzi, P.F. (1994) Cation partitioning and substitution mechanism in 1M phlogopite: a crystal chemical study. American Mineralogist, 79, 289–301.

Denner, W., Schultz, H., and D'Amour, H. (1978) A new measuring procedure for data collection with a high-pressure cell on an X-ray four-circle diffractometer. Journal of Applied Crystallography, 11, 260–264.

Ferraris, G. and Ivaldi, G. (2002) Structural features of micas. In A. Mottana, F.P. Sassi, J.B. Thompson, Jr., S. Guggenheim, Eds., Micas: Crystal Chemistry and Metamorphic Petrology. Reviews in Mineralogy and Geochemistry, 46, 117–153. The Italian National Academy, the Geochemical Society, and the Mineralogical Sociey of America, Washington, D.C.

Finger, L.W. and King, H. (1978) A revised method of operation of the single-crystal diamond cell and refinement of the structure of NaCl at 32 kbar. American Mineralogist, 63, 337–342.

Gasparik, T. (1984) Experimental study of subsolidus phase relations and mixing properties of pyroxene in the system $CaO$-$Al_2O_3$-$SiO_2$. Geochimica et Cosmochimica Acta, 48, 2537–2545.

Griffen, D.T. (1992) Silicate Crystal Chemistry. Oxford University Press. New York, Oxford.

Guven, N. (1971) The crystal structure of $2M_1$ phengite and $2M_1$ muscovite. Zeitschrift für Kristallographie, 134, 195–212.

Hazen, R.M. and Finger, L.W. (1978) The crystal structures and compressibili-

ties of layer minerals at high pressure II: Phlogopite and chlorite. American Mineralogist, 63, 293–296.
Hermann, J. (2002) Experimental constraints on phase relations in subducted continental crust. Contributions to Mineralogy and Petrology, 143, 219–235.
Holland, T.J.B. and Powell, R. (1998) An internally consistent data set for phases of petrological interest. Journal of Metamorphic Geology, 16, 309–343.
Ibers, J.A. and Hamilton, W.C., Eds. (1974) International Tables for X-ray Crystallography, 4, 99–101. Kynoch, Birmingham, U.K.
Kincaid, C. and Sacks, I.S. (1997) Thermal and dynamical evolution of the upper mantle in subduction zones. Journal of Geophysical Research, 102, 12295–12315.
Konzett, J. and Ulmer, P. (1999) The stability of hydrous potassic phases in lherzolitic mantle – an experimental study to 9.5 GPa in simplified and natural bulk compositions. Journal of Petrology, 40, 629–652.
Pavese, A., Levy, D., Curetti, N., Diella, V., Fumagalli P., and Sani, A. (2003) Equation of state and compressibility of phlogopite by in-situ high-pressure X-ray powder diffraction experiments. European Journal of Mineralogy, 15, 455–463.
Sato, K., Katsura, T., and Ito, E. (1997) Phase relations of natural phlogopite with and without enstatite up to 8 GPa: implication for mantle metasomatism. Earth and Planetary Science Letters 146, 511–526.
Sheldrick, G.M. (1997) SHELX-97. Program for crystal structure determination. University of Gottingen, Germany.
Sudo, A. and Tatsumi, Y. (1990) Phlogopite and K-amphibole in the upper mantle: implication for magma genesis in the subduction zones. Geophysical Research Letters, 17, 29–32.
Trønnes, R.G. (2002) Stability range and decomposition of potassic richterite and phlogopite end members at 5-15 GPa. Mineralogy and Petrology, 74, 129–148.
Tutti, F., Dubrovinsky, L.S., and Nygren, M. (2000) High-temperature study and thermal expansion of phlogopite. Physics and Chemistry of Minerals, 27, 599–603.
van Roermund, H.L.M., Carswell, D.A., Drury, M.R., and Heijboer, T.C. (2002) Microdiamonds in a megacryst garnet websterite pod from Bardane on the island of Fjørtoft, western Norway: Evidence for diamond formation in mantle rocks during deep continental subduction. Geology, 30, 959–962.
Wunder, B. and Melzer, S. (2002) Interlayer vacancy characterization of synthetic phlogopitic micas by IR spectroscopy. European Journal of Mineralogy, 14, 1129–1138.

MANUSCRIPT RECEIVED JULY 14, 2003
MANUSCRIPT ACCEPTED OCTOBER 20, 2003
MANUSCRIPT HANDLED BY ALESSANDRO GUALTIERI